Crystallographic Analysis of the Interaction of Nitric Oxide with Quaternary-T Human Hemoglobin[†,‡]

Nei-Li Chan,[§] Jeffrey S. Kavanaugh, Paul H. Rogers, and Arthur Arnone*

Department of Biochemistry, College of Medicine, The University of Iowa, Iowa City, Iowa 52242

Received July 14, 2003; Revised Manuscript Received November 3, 2003

ABSTRACT: In addition to interacting with hemoglobin as a heme ligand to form nitrosylhemoglobin, NO can react with cysteine sulfhydryl groups to form *S*-nitrosocysteine or cysteine oxides such as cysteinesulfenic acid. Both modes of interaction are very sensitive to the quaternary structure of hemoglobin. To directly view the interaction of NO with quaternary-T deoxyhemoglobin, crystallographic studies were carried out on crystals of deoxyhemoglobin that were exposed to gaseous NO under a variety of conditions. Consistent with previous spectroscopic studies in solution, these crystallographic studies show that the binding of NO to the heme groups of crystalline wild-type deoxyhemoglobin ruptures the Fe−proximal histidine bonds of the α-subunits but not the *β*-subunits. This finding supports Perutz's theory that ligand binding induces tension in the α Fe−proximal histidine bond. To test Perutz's theory, deoxy crystals of the mutant hemoglobin *β*W37E were exposed to NO. This experiment was carried out because previous studies have shown that this mutation greatly reduces the quaternary constraints that oppose the ligand-induced movement of the α-heme Fe atom into the plane of the porphyrin ring. As hypothesized, the Fe−proximal histidine bonds in both the *β*- and the α-subunits remain intact in crystalline *β*W37E after exposure to NO. With regard to *S*-nitrosocysteine or cysteine oxide formation, no evidence for the reaction of NO with any cysteine residues was detected under anaerobic conditions. However, when deoxyhemoglobin crystals are first exposed to air and then to NO, the appearance of additional electron density indicates that Cys93(F9)*β* has been modified, most likely to cysteinesulfenic acid. This modification of Cys93(F9)*β* disrupts the intrasubunit salt bridge between His146(HC3)*β* and Asp94(FG1)*β*, a key feature of the quaternary-T hemoglobin structure. Also presented is a reanalysis of our previous crystallographic studies [Chan, N.-L., et al. (1998) *Biochemistry 37*, 16459−16464] of the interaction of NO with liganded hemoglobin in the quaternary-R2 structure. These studies showed additional electron density at Cys93-(F9)*β* that was consistent with an NO adduct. However, for reasons discussed in this paper, we now believe that this adduct may be the Hb−S−N•−O−H radical intermediate and not Hb−S−N═O as previously suggested.

The stereochemistry of the interaction of NO with hemoglobin is complex because NO can serve as a heme ligand as well as form covalent adducts with Cys93(F9)*β*. With regard to heme ligation, previous research (*1*−*3*) has shown that the quaternary structure of nitrosylhemoglobin can be switched from the quaternary-R[e] ensemble[1] to the quaternary-T structure by addition of the potent allosteric effector inositol hexaphosphate (IHP).[2] Moreover, these studies demonstrated that this transition is accompanied by the rupture of the bond between the α-heme Fe atom and the N[ε] atom of the proximal histidine [i.e., the Fe−N[ε]His87-(F8)α bond] (*1*−*3*). In contrast, the corresponding *β*-subunit bond [Fe−N[ε]His92(F8)*β*] is not broken by IHP-induced quaternary switching (i.e., the *β*-heme maintains normal six-coordinate octahedral geometry in the nitrosylhemoglobin−IHP complex). This finding provided convincing evidence for Perutz's theory that ligation of quaternary-T hemoglobin is opposed by tension at the α-heme groups (*8*−*11*). Direct crystallographic observation of ligand-induced rupture of the Fe−N[ε]His87(F8)α bond was first reported in a structure of quaternary-T cyanomethemoglobin (*12*). The X-ray diffraction studies reported in this paper now show that the rupture of the Fe−N[ε]His87(F8)α bond occurs in crystals of wild-type deoxyhemoglobin after exposure to NO.

[†] This work was supported by National Institutes of Health Program Project Grant GM-58890. N.-L.C. was supported by a fellowship from the Iowa Affiliate of the American Heart Association.

[‡] Refined coordinates and structure factors have been deposited in the Protein Data Bank (PDB codes are 1RQ3, 1RPS, 1RQ4, and 1RQA for deoxyhemoglobin, anaerobic nitrosylhemoglobin, aerobic nitrosylhemoglobin, and anaerobic *β*W37E nitrosylhemoglobin, respectively).

* Correspondence should be addressed to this author (e-mail: arthur-arnone@uiowa.edu).

[§] Current address: Institute of Biochemistry, College of Life Science, National Chung Hsing University, Taichung City, Taiwan.

[1] Recent crystallographic studies have shown that fully liganded hemoglobin adopts an ensemble of energetically accessible structures (*4*). The structures in this ensemble are spatially distributed over a range that varies between the quaternary-R (*5*) and quaternary-R2 (*6*) conformations. The symbol R[e] refers to this ensemble. Very recent NMR experiments have shown that the quaternary structure of liganded hemoglobin in solution also is best represented by an ensemble of low-energy conformations with the average structure midway between the R and R2 conformations (*7*).

[2] Abbreviations: SNO-nitrosylhemoglobin, *S*-nitrosonitrosylhemoglobin A; GSNO, *S*-nitrosoglutathione; Δ_{24}, averaged atomic displacement of heme atoms to the 24-atom mean porphyrin plane; IHP, inositol hexaphosphate.

10.1021/bi030172j CCC: $27.50
Published on Web 12/12/2003

The basis for Perutz's theory is that the formation of the quaternary-T hemoglobin tetramer from two $\alpha\beta$ dimers creates constraints at the dimer−dimer interface that resist the ligand-induced movement of the α-heme Fe atom into the plane of the porphyrin ring. This resistance results in ligand-induced tension in a portion of the liganded T structure that includes the Fe−N$^{\epsilon}$His87(F8)α bond. Recently, it has been shown that some mutations at residue Trp37(C3)β greatly diminish the quaternary constraints and result in quaternary-T structures that have high ligand affinity (*13*−*17*). The βW37E mutation is a particularly disruptive mutation that results in tetramers that bind ligand noncooperatively with very high affinity. We hypothesized, therefore, that ligand-induced tension should not occur in βW37E hemoglobin and, therefore, that the Fe−N$^{\epsilon}$His87(F8)α bond should not rupture when crystals of βW37E deoxyhemoglobin are exposed to NO. As reported below, the results of this experiment fully support our hypothesis.

With regard to the interaction of NO with Cys93(F9)β, Stamler and co-workers (*18*−*20*) have shown that this residue can be S-nitrosylated to form *S*-nitrosohemoglobin (SNO-hemoglobin). Moreover, the formation of SNO-hemoglobin occurs much more readily in liganded hemoglobin than in deoxyhemoglobin (*18*, *21*, *22*). These observations have very important physiological implications because they suggest a possible, albeit controversial, mechanism of blood flow regulation in which the deoxygenation of hemoglobin results in the release of NO and the subsequent NO-induced dilation of blood vessels (*20*, *23*−*25*). A previous crystallographic study of quaternary-R2 carbonmonoxyhemoglobin exposed to NO under anaerobic conditions provided the first direct image of an NO adduct of Cys93(F9)β and showed that this modification of Cys93(F9)β displaces the COOH-terminal dipeptide of each β-subunit (*26*). In this paper we report complementary crystallographic studies for the quaternary-T structure of hemoglobin.

EXPERIMENTAL PROCEDURES

Preparation of Crystalline Quaternary-T Nitrosylhemoglobin. Using the batch method described previously (*27*, *28*), wild-type and βW37E deoxyhemoglobin crystals were grown at room temperature under anaerobic conditions using dithionite as a reducing agent. Specifically, well-formed crystals were grown at pH 7.0 from solutions composed of 10 mg/mL human hemoglobin, 10 mM potassium phosphate, 100 mM potassium chloride, 10−12% poly(ethylene glycol) 6000 (PEG), and 3 mM sodium dithionite.

Before exposure to NO, both wild-type and βW37E deoxyhemoglobin crystals were first soaked in a stabilizing substitute mother liquor as follows. Single crystals were placed in 2 mL septum vials and soaked for 20 min in 0.5 mL of a deoxygenated substitute mother liquor that consisted of 10 mM potassium phosphate at pH 7.0, 100 mM potassium chloride, 20% PEG, and 10 mM ascorbate. The dithionite reducing agent was replaced by ascorbate because dithionite readily reacts with NO (*29*). Next the screw-top septum vials were flushed with 3 cm^3 of gaseous NO, and the crystals were allowed to soak for 1 day before being mounted in quartz capillary tubes for data collection. Before the capillary tubes were sealed, they were flushed with an additional 3 cm^3 of gaseous NO. All of these procedures were carried out under an atmosphere of pure nitrogen. Under these conditions quaternary-T nitrosylhemoglobin was formed, but despite the high concentration of NO used in this experiment (nearly 1 atm) no reaction between NO and Cys93(F9)β was observed (i.e., SNO-hemoglobin was not formed).

Attempts To Prepare Crystalline Quaternary-T SNO-Hemoglobin under Anaerobic Conditions. The failure to observe the formation of SNO-hemoglobin may have been due to the lack of an electron acceptor or to the presence of the ascorbate reducing agent. Several studies have reported that S-nitrosylation with gaseous NO requires an electron acceptor such as O_2 or NAD^+ (*30*−*32*). However, our previous crystallographic study of crystalline carbonmonoxyhemoglobin exposed to NO under anaerobic conditions showed that NO can react with Cys93(F9)β in the absence of an obvious electron acceptor (*26*). Since the previous study was carried out under anaerobic conditions without a reducing agent, an analogous experiment was carried out using quaternary-T deoxyhemoglobin crystals. Specifically, wild-type deoxyhemoglobin crystals were exposed to gaseous NO in a substitute mother liquor that did not contain a reducing agent. However, difference electron density analysis using data collected from these crystals still showed no evidence of a reaction between NO and Cys93(F9)β. Next, we repeated this experiment with the addition of 10 mM NAD^+. Once again, no evidence of a reaction between NO and Cys93(F9)β was detected.

It has been reported that *S*-nitrosoglutathione (GSNO) can specifically react with Cys93(F9)β through a transnitrosation reaction (*18*). Therefore, we attempted to generate crystalline SNO-deoxyhemoglobin by soaking wild-type deoxyhemoglobin crystals in the substitute mother liquor described above with the addition of 15 mM GSNO. However, a 2.6 Å difference electron density map of the GSNO-treated hemoglobin versus native deoxyhemoglobin did not reveal the presence of SNO-Cys93(F9)β or any oxidized form of Cys93(F9)β. Instead, the difference map showed that under the conditions of this experiment quaternary-T nitrosylhemoglobin is produced. During the 18 h soaking period, the GSNO apparently decomposed to glutathione and gaseous NO that then bound to all four heme groups.

Attempts To Prepare Crystalline Quaternary-T SNO-Hemoglobin under Aerobic Conditions. Carrying out the S-nitrosylation reaction under aerobic conditions is complicated by the tendency of deoxyhemoglobin crystals to disorder in the presence of oxygen (*33*). However, disordering does not occur in the isomorphous crystal form of the deoxyhemoglobin−IHP complex. Exposing crystals of the deoxyhemoglobin−IHP complex to atmospheric oxygen results in the formation of partially oxidized hemoglobin in the quaternary-T structure. Specifically, under these conditions, the intermediate $\alpha(Fe^{3+}\cdot H_2O)_2\beta(Fe^{2+})_2$ is the major ligation species formed (*34*), and no oxidation of Cys93(F9)β is observed in a 2.1 Å electron density map (data not shown). Therefore, these crystals provide a means of carrying out the S-nitrosylation reaction under aerobic conditions.

Crystals of the wild-type deoxyhemoglobin−IHP complex were grown in an atmosphere of pure nitrogen from solutions of 10 mg/mL human hemoglobin, 10 mM potassium phosphate, 100 mM potassium chloride, 10−12% poly(ethylene glycol) 6000 (PEG), 0.62 mM ferrous chloride, and 3.1 mM IHP at pH 7.0. A single well-formed crystal

Table 1: Data Collection and Refinement Statistics[a]

	quaternary-T NO-hemoglobin (anaerobic)	quaternary-T NO-hemoglobin (aerobic)	quaternary-T βW37E NO-hemoglobin (anaerobic)
Data Collection			
space group	$P2_12_12$	$P2_12_12$	$P2_12_12$
unit cell			
a (Å)	97.0	97.2	95.3
b (Å)	99.3	100.4	97.8
c (Å)	66.1	66.2	66.8
asymmetric unit	tetramer	tetramer	tetramer
resolution (Å)	2.15 (2.32−2.15)	2.11 (2.27−2.11)	2.11 (2.27−2.11)
measurements	228410 (15236)	232434 (16661)	236515 (16855)
unique reflections	34068 (5934)	36755 (6499)	35916 (6537)
completeness (%)	96.9 (85.9)	96.9 (87.1)	98.0 (90.5)
av I/σ(I)	9.8 (1.9)	8.1 (1.5)	9.6 (2.0)
av multiplicity	6.7 (2.6)	6.3 (2.6)	6.6 (2.6)
R_{merge} (%)	8.7 (25.4)	9.4 (27.2)	8.5 (23.1)
REFMAC5 Refinement			
R_{cryst}	0.181 (0.236)	0.197 (0.277)	0.188 (0.234)
R_{free}	0.232 (0.284)	0.241 (0.319)	0.231 (0.274)
rms bond lengths (Å)	0.022	0.021	0.023
rms angles (deg)	1.63	1.51	2.33
av temp factor (Å^2)	28.1	26.8	26.2

[a] Values in parentheses are for the highest resolution shell of data.

was mounted in a quartz capillary tube in air, sealed, and allowed to equilibrate for 3 days. Then the capillary tube was opened in a glovebag filled with nitrogen, and a syringe was used to flush the capillary with 3 cm^3 of NO before the capillary tube was resealed. The crystal was allowed to equilibrate under these conditions for 7 days before data collection was initiated, during which time nitrosylation of the hemes took place (reductive nitrosylation in the case of the oxidized hemes). In addition, and in contrast to the results obtained under anaerobic conditions, a 2.1 Å difference electron density map of the hemoglobin exposed to NO under aerobic conditions versus native deoxyhemoglobin, or versus hemoglobin exposed to NO under anaerobic conditions, clearly showed that Cys93(F9)β had reacted with NO.

Data Collection. The diffraction data were collected at room temperature using Cu Kα radiation with a Rigaku AFC6 four-circle diffractometer fitted with a San Diego Multiwire Systems area detector. Data sets were scaled and merged using the software and procedures described by Howard et al. (*35*). Data collection and refinement statistics are summarized in Table 1.

Refinement of the Anaerobic Quaternary-T Nitrosylhemoglobin Structure. The starting model for the quaternary-T nitrosylhemoglobin refinement was our previously reported deoxyhemoglobin structure (*28*) (which had been refined with X-PLOR (*36*) and PROLSQ (*37*)) after additional refinement was carried out with the maximum-likelihood refinement program REFMAC5 (*38*, *39*). This atomic model was then refined against the quaternary-T nitrosylhemoglobin diffraction data using the X-PLOR program to carry out rigid-body refinement. First the $\alpha_2\beta_2$[3] hemoglobin tetramer, then the two $\alpha\beta$ dimers, and finally the individual α- and β-subunits underwent rigid-body refinement. The rigid-body refinement was followed by atomic refinement with REFMAC5. However, before the REFMAC5 refinement was initiated, the proximal histidines of the α-subunits were converted to alanine residues because it was clear from initial difference electron density analysis that the Fe−N$^{\epsilon}$His87(F8)α bonds were ruptured. Following REFMAC5 refinement, $2F_o - F_c$ and $F_o - F_c$ electron density maps were used with the TOM/FRODO software (*40*, *41*) to position the proximal histidine side chain of each α-subunit as well as the NO ligands of all four heme groups. In addition, an electron density peak located between His87(F8)α and Tyr140(HC2)α was modeled as a water molecule.

Refinement of the Aerobic Quaternary-T Nitrosylhemoglobin Structure. For the aerobic structure of quaternary-T nitrosylhemoglobin, a difference electron density map was calculated with $F_{\text{aerobic T nitrosylhemoglobin}} - F_{\text{anaerobic T nitrosylhemoglobin}}$ amplitudes and phases derived from the refined structure of the anaerobic quaternary-T nitrosylhemoglobin. The only features in this difference map were a positive peak next to Cys93(F9)β, indicating that it had reacted, and negative difference peaks overlapping the positions of Asp94(FG1)β and His146(HC2)β, indicating that these residues had been displaced or disordered. The refined structure of anaerobic quaternary-T nitrosylhemoglobin was used as the starting model for aerobic quaternary-T nitrosylhemoglobin. This model was subjected to rigid-body refinement with X-PLOR as described above. Residues 93β, 94β, and 146β were then converted to alanine residues and maximum-likelihood refinement was carried out with REFMAC5. Next, $2F_o - F_c$ and $F_o - F_c$ electron density maps were used with the TOM/FRODO software to position the side chains of Cys93(F9)β, Asp94(FG1)β, and His146(HC2)β. After additional REFMAC5 refinement, the extra density adjacent to Cys93(F9)β was modeled as cysteinesulfenic acid (−SOH) because the electron density envelope was not large enough to accommodate an −SNO adduct.

A molecule of IHP was not added to the aerobic quaternary-T nitrosylhemoglobin atomic model because little or no significant electron density was observed for IHP in its binding site at the entrance to the central cavity between the β-subunits. Waller and Liddington, working with the same crystal form of the deoxyhemoglobin−IHP complex, also reported very weak electron density for IHP (*34*). Since the addition of IHP prevents O_2-induced crystal disordering (*34*), IHP apparently binds to and stabilizes the quaternary-T hemoglobin tetramer. However, in this orthorhombic crystal lattice it must bind in a more disordered mode than in the monoclinic crystal lattice previously used by Arnone and Perutz to study the deoxyhemoglobin−IHP complex (*42*).

Refinement of the Anaerobic βW37E Nitrosylhemoglobin Structure. The starting model for this refinement of βW37E nitrosylhemoglobin was the βW37E deoxyhemoglobin structure (*17*) after additional refinement with REFMAC5. This starting model was refined against the anaerobic βW37E nitrosylhemoglobin diffraction data. Specifically, it was subjected to rigid-body refinement with X-PLOR (see above) followed by maximum-likelihood refinement with REFMAC5. Next $2F_o - F_c$ and $F_o - F_c$ electron density maps were used with the TOM/FRODO software to add the NO

[3] The notation $\alpha1\alpha2$, $\beta1\beta2$, $\alpha1\beta1$, $\alpha2\beta2$, $\alpha1\beta2$, and $\alpha2\beta1$ refers to the six subunit−subunit pairings within the $\alpha_2\beta_2$ hemoglobin tetramer.

ligands to all four heme groups as well as to reposition residues His87(F8)α through Arg92(FG4)α of each α-subunit. The final atomic model was obtained after additional refinement with REFMAC5 (Table 1).

Cross-Validation of Tertiary Structural Changes Using the R_{free}^{local} Parameter. An important issue in many crystallographic studies is the validation of small structural changes. To do this, we have developed a variant of the Brünger R_{free} parameter (*43*), the R_{free}^{local} parameter, that is a cross-validation statistic sensitive only to local changes in structure. The R_{free}^{local} parameter described below is a modified version of the R_{free}^{local} parameter originally described by Kavanaugh et al. (*17*).

The following example illustrates the calculation of the R_{free}^{local} parameter in the case of the cross-validation of the tertiary structural differences between anaerobic nitrosylhemoglobin and native deoxyhemoglobin. First, the native deoxyhemoglobin diffraction data were randomly divided into a test data set consisting of 10% of the data and a working data set consisting of the remaining 90% of the data. The anaerobic nitrosylhemoglobin data set also was divided into a test and a working data set, but in this case the *hkl* reflections assigned to the test data set were the same as those in the native deoxyhemoglobin test data set. The native deoxyhemoglobin atomic model was then debiased (*44*) relative to its test data set by carrying out 360 cycles of REFMAC5 refinement against its working data set. This debiased model of deoxyhemoglobin was then used as a starting model for the refinement of the anaerobic nitrosylhemoglobin structure. As described above, this refinement entailed rigid-body refinement with X-PLOR followed by REFMAC5 refinement and minor manual corrections with the TOM/FRODO software. Any global ligand-induced changes in quaternary structure that were introduced by X-PLOR rigid-body refinement could be cross-validated with the standard R_{free} parameter (*43*). However, the localized ligand-induced changes in tertiary structure that were introduced during the second stage of the refinement (the REFMAC5 and TOM/FRODO refinement) were cross-validated through the use of "hybrid" atomic models. Specifically, after convergence of the final REFMAC5 refinement cycles, hybrid atomic models were generated by replacing the coordinates of each pentapeptide in the final REFMAC5 refined model with the coordinates of the corresponding pentapeptide of the atomic model that had undergone only rigid-body refinement (but not individual atom refinement). Thus 281 hybrid atomic models were generated (137 α-chain models and 142 β-chain models). The coordinates for each of these hybrid models were identical to those of the final refined model except for a single (unrefined) pentapeptide. The R_{free} value calculated with a particular hybrid model minus the R_{free} value calculated with the final atomic model was defined as the $R_{free}^{local-5}$ value associated with the replaced pentapeptide.

$R_{free}^{local-5}$ magnitudes cannot be large because the replacement of 10 residues (e.g., Val1α1 through Ala5α1 and Val1α2 through Ala5α2) out of 574 residues represents only 1.7% (on average) of the refined model. However, if the structural changes associated with a particular pentapeptide represent a genuine improvement to the starting model, the corresponding $R_{free}^{local-5}$ value should be significantly greater than zero. Therefore, the $R_{free}^{local-5}$ value is a statistic that is sensitive only to structural changes in a particular peptide, and it can be used to discriminate between small genuine structural changes and changes in the atomic model that are due to experimental uncertainty (i.e., uncertainty associated with poorly defined regions of the electron density map). In general, any size peptide can be used to calculate $R_{free}^{local-n}$ values. However, if the peptide size is very small, the $R_{free}^{local-n}$ magnitude may not be significant, and if the peptide size is very large, spatial resolution is sacrificed. In this study, pentapeptides were used because they provided the best compromise between resolution and magnitude.

When the individual $R_{free}^{local-5}$ values are plotted versus residue number, a $R_{free}^{local-5}$ profile is generated that can be compared with a corresponding profile of the $rmsd_5$ tertiary structure differences (see below) between the two structures being analyzed. Peaks in the $R_{free}^{local-5}$ profile identify (cross-validate) significant differences in tertiary structure. In the case of the comparison of anaerobic nitrosylhemoglobin versus native deoxyhemoglobin, almost all of the major ligand-induced changes in tertiary structure were cross-validated by a single $R_{free}^{local-5}$ profile. However, a single $R_{free}^{local-5}$ profile failed to cross-validate a few small changes in tertiary structure despite the fact that these structural changes were observed in both $\alpha\beta$ dimers. We then realized that we could greatly improve the sensitivity of the $R_{free}^{local-5}$ parameter by carrying out multiple calculations with different, mutually exclusive, test data sets. That is, the $R_{free}^{local-5}$ calculation was repeated ten times. In each case, the calculation started with a deoxyhemoglobin model that had been debiased relative to one of ten mutually exclusive test data sets. Averaging the resulting $R_{free}^{local-5}$ profiles allows us to use all of the diffraction data to cross-validate tertiary structural changes.

Structural Analysis. To identify ligand-induced changes in tertiary structure, corresponding subunits of deoxyhemoglobin and nitrosylhemoglobin were superimposed using an iterative least-squares superposition ("sieve-fit") procedure (*4*, *17*) similar to that described by Gerstein and Chothia (*45*). Changes in tertiary structure were identified by calculating the root-mean-square deviation (rmsd) of all the atoms (backbone plus side chain atoms) for each pair of corresponding pentapeptides in the superimposed structures. This statistic, referred to as $rmsd_5$, is plotted versus residue number to generate a profile of the five-residue-averaged tertiary structure changes. A five-residue window was selected so that the $rmsd_5$ values corresponded with the $R_{free}^{local-5}$ values (above).

RESULTS

Analysis of Heme Stereochemistry. Consistent with earlier spectroscopic studies (*1*−*3*, *46*, *47*), the crystal structure of quaternary-T nitrosylhemoglobin clearly reveals that nitrosylation of the heme groups ruptures the Fe−N$^{\epsilon}$His87(F8)α bond but not the Fe−N$^{\epsilon}$His92(F8)β bond. Continuous electron density can be seen between the α Fe and the proximal histidine side chain in the deoxyhemoglobin electron density map (Figure 1a), but there is a clear absence of electron density in the corresponding region of the nitrosylhemoglobin electron density map (Figure 1b). In the

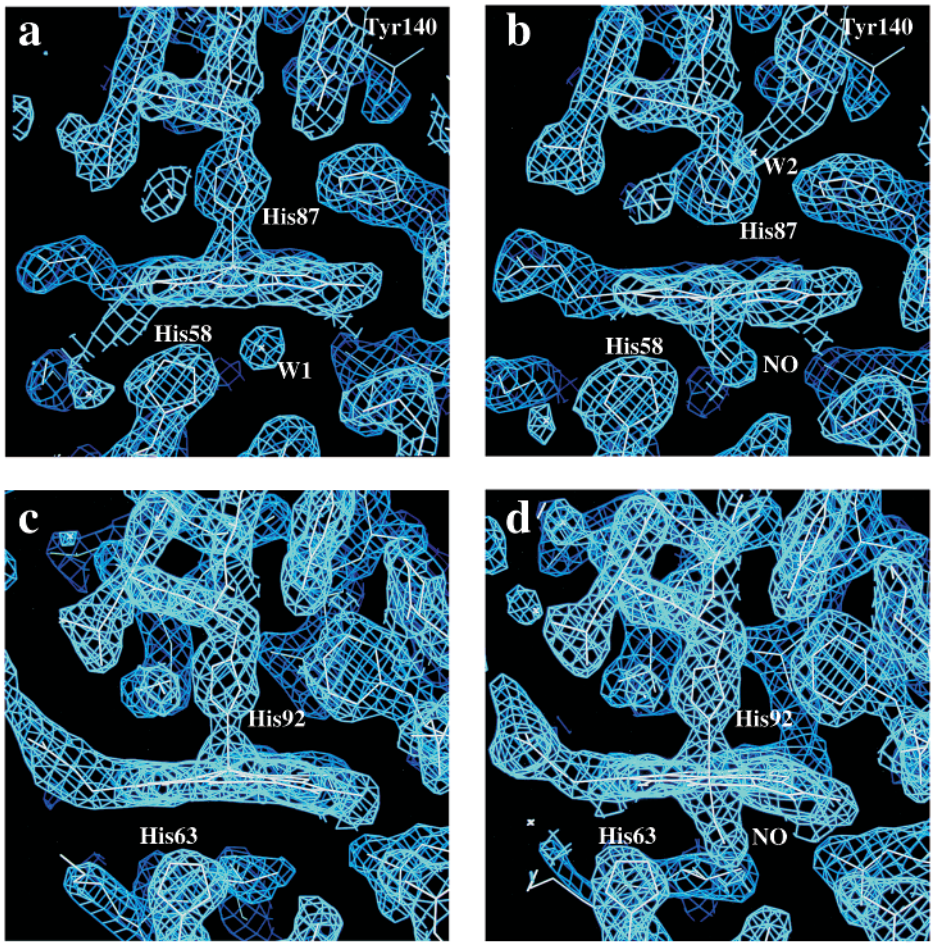

FIGURE 1: $2F_o - F_c$ electron density maps showing the environment of heme groups for the (a) α1-subunit of deoxyhemoglobin, (b) α1-subunit of quaternary-T nitrosylhemoglobin, (c) β1-subunit of deoxyhemoglobin, and (d) β1-subunit of quaternary-T nitrosylhemoglobin. Proximal histidines, heme groups, and NO molecules were not included in the atomic model used to calculate the F_c structure factor magnitudes and phases. The electron density contours are drawn at 1.6 times the rms density of the map.

refined atomic model of quaternary-T nitrosylhemoglobin, the distance between the α Fe atom and the N^{ϵ} atom of His87(F8)α is 4.06 Å. Therefore, it can be concluded that the Fe−N^{ϵ}His87(F8)α bond no longer exists in the quaternary-T nitrosylhemoglobin tetramer.

The β-heme groups of quaternary-T nitrosylhemoglobin respond very differently to the binding of NO. Continuous electron density is observed between the β Fe and the proximal histidine in both the deoxyhemoglobin and nitrosylhemoglobin electron density maps (Figure 1c,d), clearly showing that the Fe−N^{ϵ}His92(F8)β bond remains intact after NO binds to crystalline deoxyhemoglobin. Consequently, the β-heme groups in quaternary-T nitrosylhemoglobin are six-coordinate with both NO and the imidazole group of the proximal histidine serving as axial ligands. The average Fe−N^{ϵ}His92(F8)β bond length is 2.25 Å in the refined structure of quaternary-T nitrosylhemoglobin, a distance that agrees well with those reported in other crystallographic studies (Table 2), and one that is consistent with the presence of a trans axial Fe−NO bond (*48*).

The α-heme groups of quaternary-T nitrosylhemoglobin exhibit significant conformational differences relative to their structures in deoxyhemoglobin. In each α-subunit, nitrosylation results in a flattening of the heme group (as indicated by a decrease of the out-of-plane rms distance of the atoms in the 24-atom porphyrin plane, Δ_{24}) and in the movement of the Fe atom toward the distal side of the porphyrin plane (see Table 2). Specifically with regard to heme flattening, the Δ_{24} values for the α-heme groups in deoxyhemoglobin (*28*) and quaternary-T nitrosylhemoglobin are 0.185 and 0.126 Å, respectively. With regard to the movement of the α Fe atom, the five-coordinate α Fe in deoxyhemoglobin is positioned out of the 24-atom porphyrin plane toward the proximal histidine by 0.59 Å, whereas the five-coordinate α Fe atom in quaternary-T nitrosylhemoglobin is 0.25 Å out of the porphyrin plane toward the distal heme pocket. Thus the α Fe moves by ~0.84 Å from the proximal side to the distal side of the heme plane in response to the binding of NO and the rupture of the Fe−N^{ϵ}His87(F8)α bond. The out-of-plane distance of the α Fe in quaternary-T nitrosylhemoglobin is in very good agreement with the distance reported in a five-coordinate nitrosylmetalloporphyrin model compound (Table 2).

In the case of the β-subunits, the heme groups do not flatten in response to NO binding. The Δ_{24} values for the β-heme groups in deoxyhemoglobin (*28*) and quaternary-T nitrosylhemoglobin are 0.183 and 0.174 Å, respectively. The geometry of the six-coordinate β nitrosylhemes is similar to that observed in other nitrosylated hemoproteins as well as in six-coordinate nitrosylmetalloporphyrin model compounds (Table 2). In deoxyhemoglobin the β Fe atom is 0.42 Å out of the heme plane toward the proximal side. In quaternary-T

Table 2: Heme−Ligand Stereochemistry in Various Crystal Structures

structure[a,b]	Fe−HisN$^{\epsilon 2}$ (Å)	Fe−N (Å)	N−O (Å)	Fe−N−O (deg)	Fe out-of-heme-plane[c] (Å)
Fe^{II}(NO)TPP		1.72	1.12	149	0.21
Fe^{II}(NO)TPP(1-MeIm)	2.18	1.74	1.14, 1.12[d]	138, 142[d]	0.05
nitrosylleghemoglobin	2.20	1.72	1.22	147	−0.01
nitrosylmyoglobin	2.18	1.89	1.15	112	0.00
quaternary-R2 SNO-nitrosylHb[e]	2.28, 2.28	1.75, 1.74	1.13, 1.11	131, 123	−0.03, −0.05
quaternary-T deoxyHb[e]	2.23, 2.22				−0.59, −0.42
quaternary-T nitrosylHb, anaerobic[e]	4.06,[f] 2.25	1.72, 1.75	1.13, 1.15	138, 128	0.25, −0.12
quaternary-T nitrosylHb, aerobic[e]	4.20,[f] 2.19	1.72, 1.76	1.15, 1.17	138, 138	0.22, −0.14
quaternary-T nitrosyl βW37E[e]	2.24, 2.19	1.71, 1.76	1.16, 1.18	135, 126	−0.15, −0.02

[a] Abbreviations: TPP, tetraphenylporphyrin; 1-MeIm, 1-methylimidazole. [b] Fe^{II}(NO)TPP (*72*); Fe^{II}(NO)TPP(1-MeIm) (*48*); nitrosylleghemoglobin (*51*); nitrosylmyoglobin (*50*); quaternary-R2 SNO-nitrosylHb (*26*); quaternary-T deoxyHb (*28*); quaternary-T nitrosylHb (this study); quaternary-T SNO-nitrosylHb (this study). [c] A negative sign indicates that the Fe is out-of-heme-plane on the proximal side of the porphyrin plane. [d] The nitric oxide oxygen atom is disordered over two positions. [e] For each tetrameric hemoglobin structure the first and second values for each parameter are the averaged values for the α-subunits and the β-subunits, respectively. The Fe−HisN$^{\epsilon 2}$ bonds and the Fe out-of-heme-plane distances were refined by adjusting the corresponding REFMAC5 target distances until they matched the refined distances (*17*). [f] Nonbonded distance between α Fe and HisN$^{\epsilon 2}$.

nitrosylhemoglobin the β Fe atom moves toward the distal side of the heme, but unlike the α Fe atom the β Fe atom remains 0.12 Å out of the plane on the proximal side.

In all four subunits of quaternary-T nitrosylhemoglobin the NO ligand adopts a slightly bent geometry. The NO oxygen atom points toward the pyrrole C ring of the heme group and away from the side chains of the distal histidine at position E7 (His58α/His63β) and the valine at position E11 (Val62α/Val67β). The averaged Fe−N−O bond lengths and bond angles for the α- and β-heme groups are in good agreement with the values observed in other nitrosylmetalloporphyrins (Table 2). In the case of the α-subunits, the NO ligand, like other heme ligands, must displace a water molecule (labeled W1 in Figure 1a) that is hydrogen-bonded to the distal histidine in deoxyhemoglobin.

The changes in heme stereochemistry and the addition of the NO ligand to the quaternary-T nitrosylhemoglobin atomic model are cross-validated by a R_{free}^{local} calculation (see Experimental Procedures). The R_{free} value for the final quaternary-T nitrosylhemoglobin atomic model is 0.232. The R_{free} value increases to 0.242 when the α-heme coordinates from the final quaternary-T nitrosylhemoglobin atomic model are replaced with the corresponding α-heme coordinates from the unliganded atomic model that had only been subjected to rigid-body refinement against the nitrosylhemoglobin diffraction data. The heme R_{free}^{local} value (0.010) for the α-subunit heme groups is the difference between these two R_{free} values. Since the heme R_{free}^{local} corresponding to the α-subunit heme groups is significantly greater than zero, the ligand-induced changes in α-subunit heme structure cross-validate. In the case of the β-subunits, the binding of NO induces a smaller movement of the iron atom toward the heme plane (0.30 Å) as well as an ~0.4 Å shift in the position of the heme group (see below). A heme R_{free}^{local} value of 0.009 for the β-subunit heme groups indicates that these changes in the stereochemistry and position of the β-heme groups also are valid.

Ligand-Induced Tertiary Structure Changes in Quaternary-T Nitrosylhemoglobin. When crystallographic methods are used to characterize small tertiary structure changes caused by mutation or the binding of ligand, a fundamental issue that should be specifically addressed is the validity of these small changes in structure. That is, it must be determined if these are genuine structural changes that are due to ligand binding or mutation or if they are simply due to small random variations in atomic positions that are to be expected in any X-ray structure determination. One way to establish the validity of a small change in structure is to demonstrate that it occurs in two or more pairs of structures that were independently determined in the same crystal lattice (i.e., by making use of noncrystallographic symmetry) or in different crystal lattices (*17*). The $R_{free}^{local-5}$ parameter (described above) provides a second, complementary approach to the verification of small changes in tertiary structure. In Figures 2 and 3 we have used both of these methods to identify valid NO-induced tertiary structure changes in the α- and β-subunits of quaternary-T hemoglobin.

Shown in Figure 2 are plots of α chain $rmsd_5$, $R_{free}^{local-5}$, and deoxyhemoglobin temperature factor (B_5) profiles where each parameter has been calculated over all overlapping five-residue windows. Figure 2a identifies two major regions of possible ligand-induced changes in tertiary structure where the α1 and α2 $rmsd_5$ profiles are in agreement. The first extends approximately from residue 43α to residue 60α, and the second extends from residue 73α to residue 101α. Within the second broad region, the α1 and α2 $rmsd_5$ profiles are very closely matched between central residues 79α−97α and much less so on the shoulders. A few other smaller $rmsd_5$ peaks occur in only the α1-subunit or the α2-subunit and are therefore less likely to represent genuine structural changes.

The $R_{free}^{local-5}$ profile in Figure 2b also identifies two regions of significant α-subunit tertiary structure change. These regions, labeled 1α and 2α, extended over residues 55α−60α and 79α−97α, respectively. Region 2α corresponds only with the central portion of the 73α −101α $rmsd_5$ peak in Figure 2a. That is, the $R_{free}^{local-5}$ parameter cross-validates the central portion 73α−101α $rmsd_5$ peak but not its shoulders. The left shoulder (residues 73α−78α) occurs only in the α2-subunit and coincides with a region of high temperature factors (Figure 2c). Thus the high $rmsd_5$ values for residues 73α2−78α2 appear to be a consequence of the inherent high mobility (i.e., the poorly defined electron density envelope) of the EF-corner of the α2-subunit, rather than a genuine structural change that is associated with NO

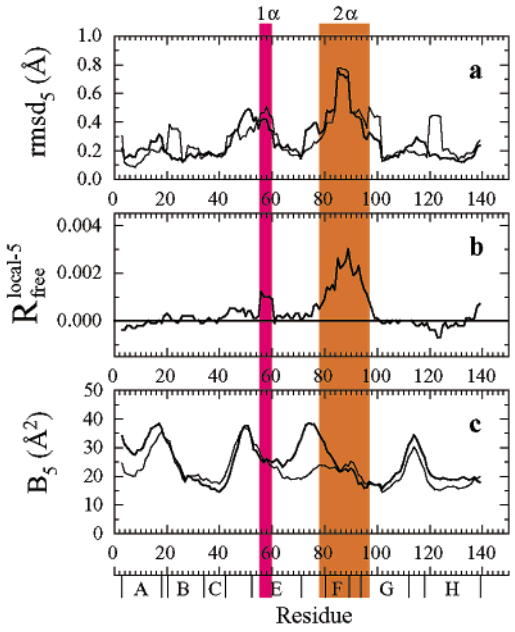

FIGURE 2: Plots of α-subunit (a) rmsd$_5$, (b) $R_{free}^{local-5}$, and (c) temperature factor (B_5) profiles where each parameter has been calculated over all overlapping five-residue windows (see text). The rmsd$_5$ parameter is the root-mean-square deviation in α-subunit atomic coordinates calculated after a quaternary-T nitrosylhemoglobin α-subunit has been superimposed via the sieve-fit protocol onto the corresponding quaternary-T deoxyhemoglobin α-subunit. The $R_{free}^{local-5}$ parameter cross-validates tertiary structure changes and is described in the text. The B_5 profiles are average atomic temperature factors for all the atoms in a given pentapeptide of the quaternary-T deoxyhemoglobin α-subunits. In panels a and c the α1- and α2-subunit profiles are drawn with thin and thick lines, respectively. The globin helical boundaries are indicated along the bottom axis. The colored bands (labeled 1α and 2α) highlight the two major $R_{free}^{local-5}$ peaks in panel b.

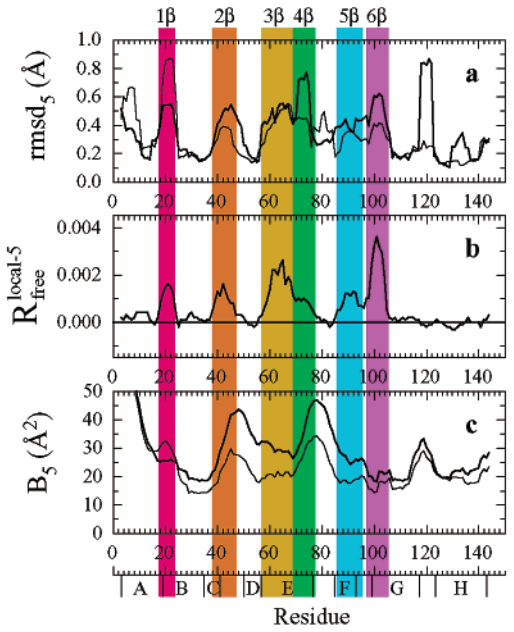

FIGURE 3: Plots of β-subunit (a) rmsd$_5$, (b) $R_{free}^{local-5}$, and (c) temperature factor (B_5) profiles where each parameter has been calculated over all overlapping five-residue windows (see text). The rmsd$_5$ parameter is the root-mean-square deviation in β-subunit atomic coordinates calculated after a quaternary-T nitrosylhemoglobin β-subunit has been superimposed via the sieve-fit protocol onto the corresponding quaternary-T deoxyhemoglobin β-subunit. The $R_{free}^{local-5}$ parameter cross-validates tertiary structure changes and is described in the text. The B_5 profiles are for the quaternary-T deoxyhemoglobin β-subunits. In panels a and c the β1- and β2-subunit profiles are drawn with thin and thick lines, respectively. The globin helical boundaries are indicated along the bottom axis. The colored bands (labeled 1β through 6β) highlight the six major $R_{free}^{local-5}$ peaks in panel b. The temperature factors for the first six pentapeptides exceed 50 Å^2 and are highest for the first pentapeptide, where the values are 82 and 85 Å^2 for β1 and β2, respectively.

binding. The temperature factors of this region of the α1-subunit are much lower because a major lattice contact limits its mobility (see Figure 4 in ref *49*). The right shoulder of the 73α−101α rmsd$_5$ peak (residues 98α−101α), which occurs in both the α1 and α2-subunits but is more prominent in the α1-subunit, is almost solely due to large movements in the side chain atoms of Lys99(G6)α. Since both Lys99(G6)α1 and Lys99(G6)α2 are almost completely disordered, the right shoulder of the 73α−101α rmsd$_5$ peak has no impact on the $R_{free}^{local-5}$ parameter and is not a consequence of ligand binding.

Region 1α (55α−60α) as identified in the $R_{free}^{local-5}$ profile (Figure 2b) is centered on the α-subunit distal histidine [His58(E7)α] and corresponds to only the COOH-terminal third of the 43α−60α rmsd$_5$ peak in Figure 2a. Region 1α is clearly due to ligand-induced movements that are the result of interactions between the NO ligand and the distal histidine. The remainder of the 43α−60α rmsd$_5$ peak also may be ligand-induced, but it does not give a clear cross-validation signal in the $R_{free}^{local-5}$ profile because it is part of the very mobile α CD-corner which has high temperature factors and, therefore, weak electron density.

Shown in Figure 3 are plots of β chain rmsd$_5$, $R_{free}^{local-5}$, and deoxyhemoglobin temperature factor (B_5) profiles. In contrast to the α-subunit rmsd$_5$ profiles, which show only two regions of ligand-induced changes in tertiary structure, the β-subunit rmsd$_5$ profiles (Figure 3a) show five narrow regions and one very broad region of possible ligand-induced movements. Three of the narrow peaks, residues 3β to 10β, 16β to 25β, and 38β to 52β, occur in both the β1 and β2 rmsd$_5$ profiles, whereas the other two narrow peaks, residues 117β to 124β and 130β to 137β, occur only in the β2 rmsd$_5$ profile. The broad peak extends over residues 57β to 107β in both β-subunit rmsd$_5$ profiles. The $R_{free}^{local-5}$ profile for the β-subunits (Figure 3b) cross-validates two of the narrow regions that occur in both β-subunits (labeled 1β and 2β) and resolves the very broad 57β to 107β rmsd$_5$ peak into five regions, four (labeled 3β, 4β, 5β, and 6β) of which cross-validate. Four rmsd$_5$ peaks do not cross-validate: 3β to 10β, 76β to 86β, 117β to 124β, and 130β to 137β. Peaks 3β to 10β and 76β to 86β (which correspond to the β NH_2 terminus and the β EF-corner) have high temperature factors (Figure 3c). The remaining rmsd$_5$ peaks (117β to 124β and 130β to 137β) only occur in the β2-subunit and are due mainly to large movements of the side chains of Lys120(GH3)β and Lys132(G10)β. However, it is interesting to note that these two rmsd$_5$ peaks also appear in other comparisons between liganded and unliganded β-subunits (see Discussion section).

In summary, NO binding induces small movements in two peptides of the α-subunits (regions 1α and 2α) and six peptides of the β-subunits (regions 1β−6β). The nature of the structural changes in the α-subunits is illustrated in Figure 4 where the α1-subunit of quaternary-T nitrosylhemoglobin

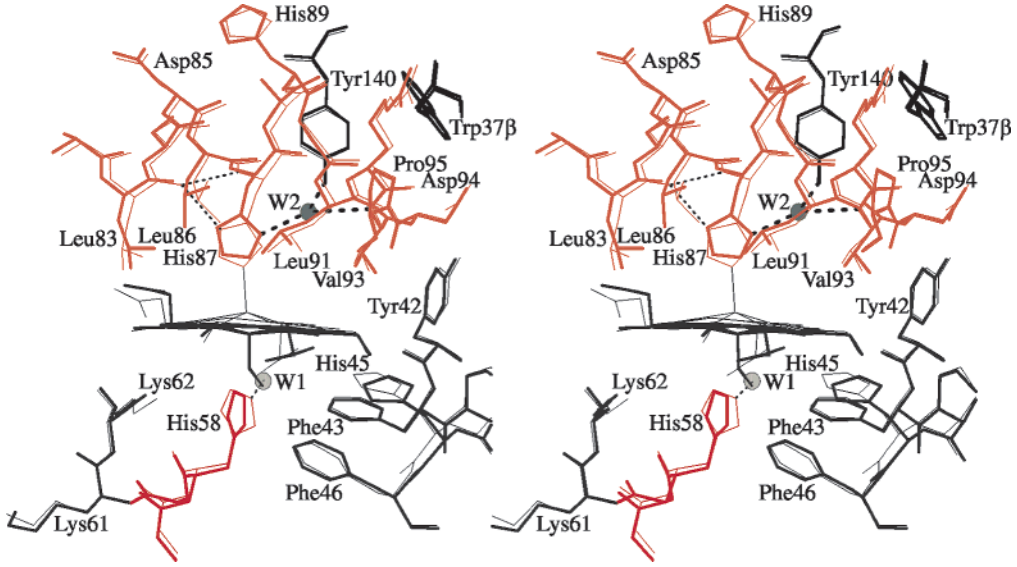

FIGURE 4: Stereo diagram showing the environment of the α1-heme group in deoxyhemoglobin (thin lines) and quaternary-T nitrosylhemoglobin (thick lines) after the α1-subunits of the two structures were superimposed using the sieve-fit procedure (see Experimental Procedures). Color coding corresponds to the polypeptide segments identified in the $R_{free}^{local-5}$ profile in Figure 2b. Hydrogen bonds are indicated by dashed lines. Bound water molecules W1 and W2 are in the deoxyhemoglobin and quaternary-T nitrosylhemoglobin structures, respectively. Trp37(C3)β2 is located at the top right.

is superimposed on the α1-subunit of deoxyhemoglobin, and the nature of the structural changes in the β-subunits is illustrated in Figure 5 where the β1-subunit of quaternary-T nitrosylhemoglobin is superimposed on the β1-subunit of deoxyhemoglobin. In Figure 4 regions 1α and 2α and in Figure 5 regions 1β through 6β are color coded as in Figures 2 and 3, respectively.

The tertiary structure changes in region 1α are about 0.4 Å in magnitude and correspond to shifts in the distal histidine, His58(E7)α, and adjacent residues. These changes appear to be due to steric contacts between the NO ligand and the distal histidine. Specifically, when the individual α-subunits of quaternary-T nitrosylhemoglobin are superimposed on the corresponding α-subunits of deoxyhemoglobin, the nitrogen and oxygen atoms of the NO ligand are 2.75 and 2.59 Å, respectively, from the N^{ϵ} of the distal histidine of the deoxyhemoglobin atomic model. (That is, these are the distal histidine−NO distances that would occur if NO bound to deoxyhemoglobin without any ligand-induced changes in tertiary structure.) These two hypothetical distances are shorter than the corresponding distances reported in high-resolution crystal structures of nitrosylmyoglobin (*50*), nitrosylleghemoglobin (*51*), and human quaternary-R2 nitrosylhemoglobin (*26*). In the refined structure of quaternary-T nitrosylhemoglobin the tertiary structure changes associated with the distal histidine and adjacent E-helix residues alter the environment of the ligand binding pocket so that the nitrogen and oxygen atoms of the NO ligand are 3.39 and 3.34 Å from the N^{ϵ} of the α distal histidine, distances very similar to those reported previously (*26*, *50*, *51*).

The tertiary structure changes in region 2α range from 0.3 to 0.8 Å in magnitude and correspond to shifts in the F-helix, the FG-corner, and the beginning of the G-helix. The largest of these changes occurs at the proximal histidine [His87(F8)α] and adjacent residues and is due to the rupture of the Fe−N^{ϵ}His87(F8)α bond. Surprisingly, when the proximal histidine is not constrained by the Fe−N^{ϵ}His87(F8)α covalent bond, its imidazole ring rotates 180° about χ_2, disrupting the hydrogen bond between its protonated N^{δ} atom and the carbonyl oxygen of Leu83(F4)α which normally is present in both deoxy and liganded hemoglobin. Instead, in quaternary-T nitrosylhemoglobin the N^{δ} atom forms a hydrogen bond with a newly recruited water molecule (W2 in Figures 1 and 4). This water is present in both α-subunits and forms intrasubunit hydrogen bonds with Tyr140(HC2)α and Val93(FG5)α.

Normally, ligand binding to the α-heme induces a small shift of the F-helix toward the FG-corner and the α1β2 interface (*52*, *53*). In contrast, NO binding and the rupture of the Fe−N^{ϵ}His87(F8)α covalent bond induces a movement of the F-helix in the opposite direction, i.e., toward the α EF-corner (Figure 4) and away from the α1β2 interface, a finding that is in agreement with the ligand-induced movements reported for the crystal structure of quaternary-T cyanomethemoglobin in which the Fe−N^{ϵ}His87(F8)α bond also is ruptured (*12*).

The differences in β-subunit tertiary structure between quaternary-T deoxyhemoglobin and quaternary-T nitrosylhemoglobin are somewhat larger, and they are distributed over a much wider range of residues than the tertiary structure differences in the α-subunits (Figure 2a versus Figure 3a). The key structural difference between the response of the β-subunits and the response of the α-subunits to the binding of NO is that a ligand-induced movement of the heme group occurs in the β-subunits but not in the α-subunits. Rigid-body analysis (*54*) of the β-heme movement reveals that it can be accurately described by a rotation of 5.1° about an axis that is perpendicular to the Fe−N^{ϵ}-His92(F8)β bond. As shown in Figure 5, this rigid-body rotation shifts the β-heme by ~0.4 Å toward the NH_2-terminal end of the G-helix [Asn102(G4)β and Phe103(G5)β] in a way that displaces pyrrole ring A toward the distal side of the heme pocket and pyrrole ring C toward the proximal side. To accommodate the ligation-induced movement of the β-heme group, residues in regions 2β, 4β, 5β, and 6β (Figure 3) shift position in order to maintain optimal packing

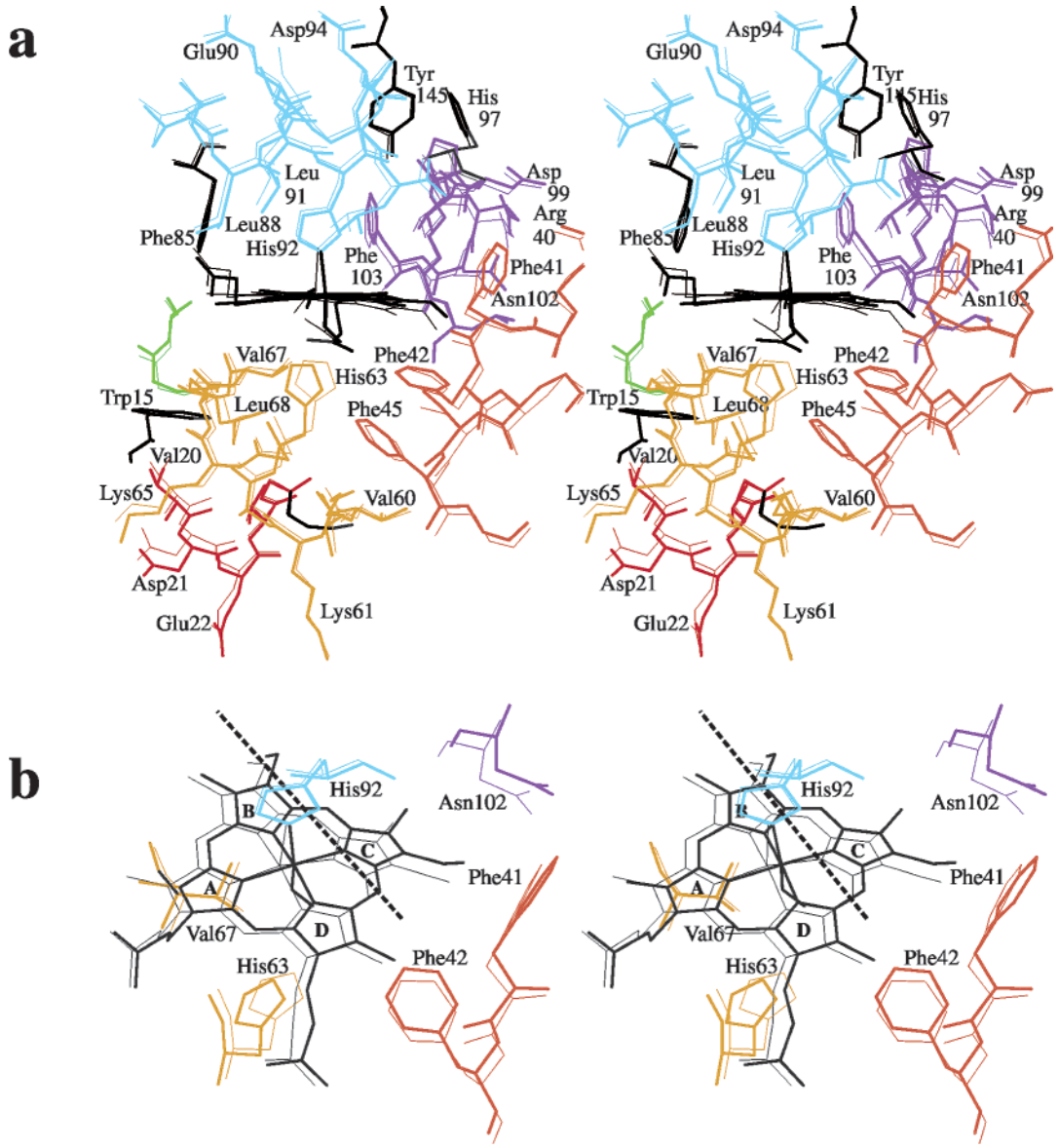

FIGURE 5: (a) Stereo diagram showing the environment of the β1-heme group in deoxyhemoglobin (thin lines) and quaternary-T nitrosylhemoglobin (thick lines) after the β1-subunits of the two structures were superimposed using the sieve-fit procedure (see Experimental Procedures). Color coding corresponds to the polypeptide segments identified in the $R_{free}^{local-5}$ profile in Figure 3b. (b) Enlarged and rotated view of the structures in (a) showing the ligand-induced movement of the β1-heme group. The dashed line locates the screw-rotation axis that describes the ligand-induced heme movement (see text). Color coding is as in Figure 3b; pyrrole rings are labeled A−D.

interactions with the heme (Figure 5). As in the α-subunits, the β distal histidine, His63(E7)β, and flanking residues (region 3β) shift position in order for the distal histidine to maintain optimal steric contacts with the NO ligand. The residues in region 1β shift because they are in direct van der Waals contact with the residues in region 3β.

The Fe−N$^{\epsilon}$His87(F8)α Bond Is Intact in the Quaternary-T Tetramer of βW37E Nitrosylhemoglobin. On the basis of his crystallographic and spectroscopic studies, Perutz theorized that the binding of ligand induces tension in a portion of the liganded T structure that includes the Fe−N$^{\epsilon}$His87(F8)α bond (*11*, *55*, *56*). Consistent with this theory is the finding that NO binding ruptures the Fe−N$^{\epsilon}$His87(F8)α bond when the hemoglobin tetramer is constrained in the quaternary-T conformation either by the allosteric effector IHP in solution (*1*−*3*) or, as described above, by crystal lattice contacts. Recent studies (*13*−*17*) have shown that the βW37E mutation disrupts quaternary constraints at the α1β2 interface in such a way as to prevent ligand-induced tension from developing in the quaternary-T structure. Together, these findings predict that NO binding should not rupture the Fe−N$^{\epsilon}$His87(F8)α bond in quaternary-T tetramers of βW37E nitrosylhemoglobin. This prediction was tested by exposing crystals of βW37E deoxyhemoglobin to NO with exactly the same protocol described above for crystals of wild-type deoxyhemoglobin. As hypothesized, the Fe−N$^{\epsilon}$His87(F8)α bond was found to be intact in the crystal structure of quaternary-T βW37E nitrosylhemoglobin. Specifically, as shown in Figure 6, electron density images clearly reveal that both the α- and β-heme groups are six-coordinate in the quaternary-T βW37E nitrosylhemoglobin crystals. The refined Fe−N$^{\epsilon}$His87(F8)α and Fe−N$^{\epsilon}$His92(F8)β bond lengths are 2.24 and 2.19 Å, respectively, consistent with values reported for other six-coordinate nitrosyl heme groups (Table 2). In addition, Tyr140(HC2)α is displaced by a large ligand-induced shift in the F-helix.

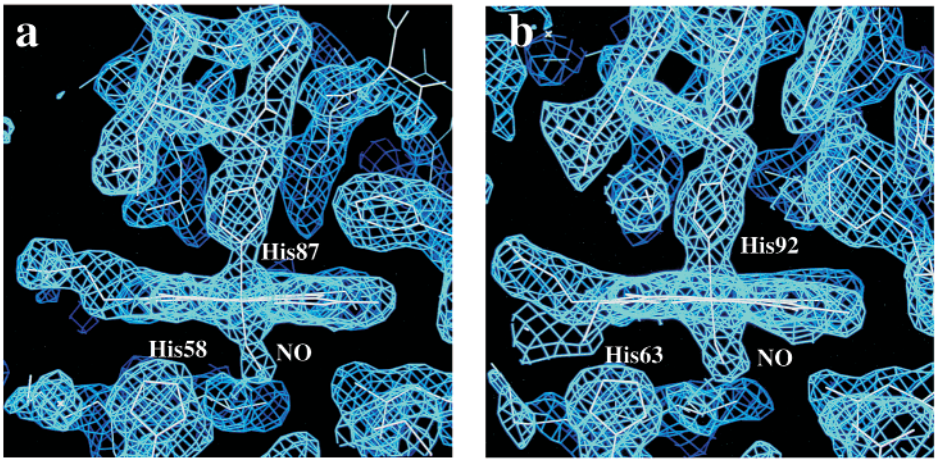

FIGURE 6: $2F_o - F_c$ electron density maps showing the environment of the heme groups for the (a) α1-subunit of quaternary-T nitrosylhemoglobin βW37E and (b) β1-subunit of quaternary-T nitrosylhemoglobin βW37E. Proximal histidines, heme groups, and NO molecules were not included in the atomic model used to calculate the F_c structure factor magnitudes and phases. The electron density contours are drawn at 1.6 times the rms density of the map. Note that the electron density for Tyr140(HC2)α (which is present in Figure 1a,b) is absent in panel a because Tyr140(HC2)α has been displaced by large NO-induced tertiary structure changes in the F-helix of quaternary-T nitrosylhemoglobin βW37E.

NO Modification of Cys93β. Exposing crystals of deoxyhemoglobin to 1 atm of NO under anaerobic conditions failed to modify any of the six cysteine residues in the quaternary-T nitrosylhemoglobin tetramer. The electron density features associated with Cys93(F9)β and the residues surrounding Cys93(F9)β in deoxyhemoglobin and in anaerobic quaternary-T nitrosylhemoglobin (panels a and b of Figure 7, respectively) are virtually identical. This is in sharp contrast to the result obtained after crystals of quaternary-R2 carbonmonoxyhemoglobin were exposed to 1 atm of NO under anaerobic conditions where high-resolution electron density images clearly revealed that Cys93(F9)β had been modified [see Figure 1 of Chan et al. (*26*)]. As described in the Experimental Procedures section, several other attempts to modify Cys93(F9)β with NO in crystals of deoxyhemoglobin (with or without the addition of an electron acceptor) also failed under anaerobic conditions. Only when deoxyhemoglobin crystals (stabilized with IHP) were first exposed to oxygen before exposure to NO did we detect evidence for the modification of Cys93(F9)β. As shown in Figure 7c, a difference electron density map of aerobic versus anaerobic NO-exposed crystals shows an increase in electron density adjacent to Cys93(F9)β and decreases in electron density associated with Asp94(FG1)β and His146(HC3)β. This indicates that under aerobic conditions Cys93(F9)β was modified in the presence of NO and that this modification disrupts the adjacent intrasubunit salt bridge between Asp94(FG1)β and His146(HC3)β. The extra electron density adjacent to Cys93(F9)β was modeled as cysteinesulfenic acid (−SOH) because the electron density envelope was not large enough to accommodate an −SNO adduct (Figure 7d). Moreover, the oxygen atom of the modeled cysteinesulfenic acid is 2.9 Å from an oxygen atom on the Asp94(FG1)β side chain, consistent with the presence of a −SOH···O hydrogen bond (Figure 7e). However, very weak additional electron density adjacent to the modeled cysteinesulfenic acid adduct indicates the possibility of a mixture of other reaction products including −SNO.

DISCUSSION

Nitric oxide forms reversible covalent bonds at two very different types of sites on the hemoglobin tetramer: the four heme−Fe sites and two of the six cysteine sulfhydryl sites. The interaction between NO and the cysteine sites, Cys93(FG1)β1 and Cys93(FG1)β2, has generated much interest and controversy because of its potential importance in the regulation of blood flow (*18*, *20*, *23*−*25*). The interaction between hemoglobin's heme groups and NO is equally interesting because it dramatically illustrates a key structural difference between the α- and β-subunits, i.e., the formation of a high level of ligand-induced tension at the Fe−N$^{\epsilon}$His87(F8)α bond in the quaternary-T structure. The crystallographic results reported above address the stereochemistry of both modes of interaction between hemoglobin and nitric oxide.

Sulfhydryl Reactivity of Cys93(F9)β in Quaternary-T Hemoglobin. Numerous solution studies have shown that an electron acceptor, such as O_2, is required for the formation of the *S*-nitroso adduct at Cys93(F9)β (*30*−*32*, *57*). The results of our current study on the reaction of NO with quaternary-T hemoglobin are consistent with the requirement for O_2 as an electron acceptor in that no evidence for the reaction of Cys93(F9)β was detected at very high NO concentration (pNO ∼1 atm) in the absence of O_2. The experimental procedure that successfully modified Cys93(F9)β involved the exposure of IHP-stabilized deoxyhemoglobin crystals to air prior to exposure to NO. Since under these conditions crystalline hemoglobin exists predominantly as the partially oxidized species $\alpha(Fe^{3+}\cdot H_2O)_2\beta(Fe^{2+})_2$ (*34*), our results are also consistent with the role of heme−Fe(III) in the redox activation of NO (*32*). Alternatively, since the mother liquor of our deoxyhemoglobin−IHP crystals contained ferrous chloride as a reducing agent, ferric ions formed after exposure to air also may have served as an electron acceptor. The electron density envelope associated with the modified Cys93(F9)β residue in these crystals, however, appears to be most consistent with cysteinesulfenic acid (Cys-SOH) and, perhaps, with minor amounts of *S*-nitrosocysteine. It is significant to note that the only other crystallographic

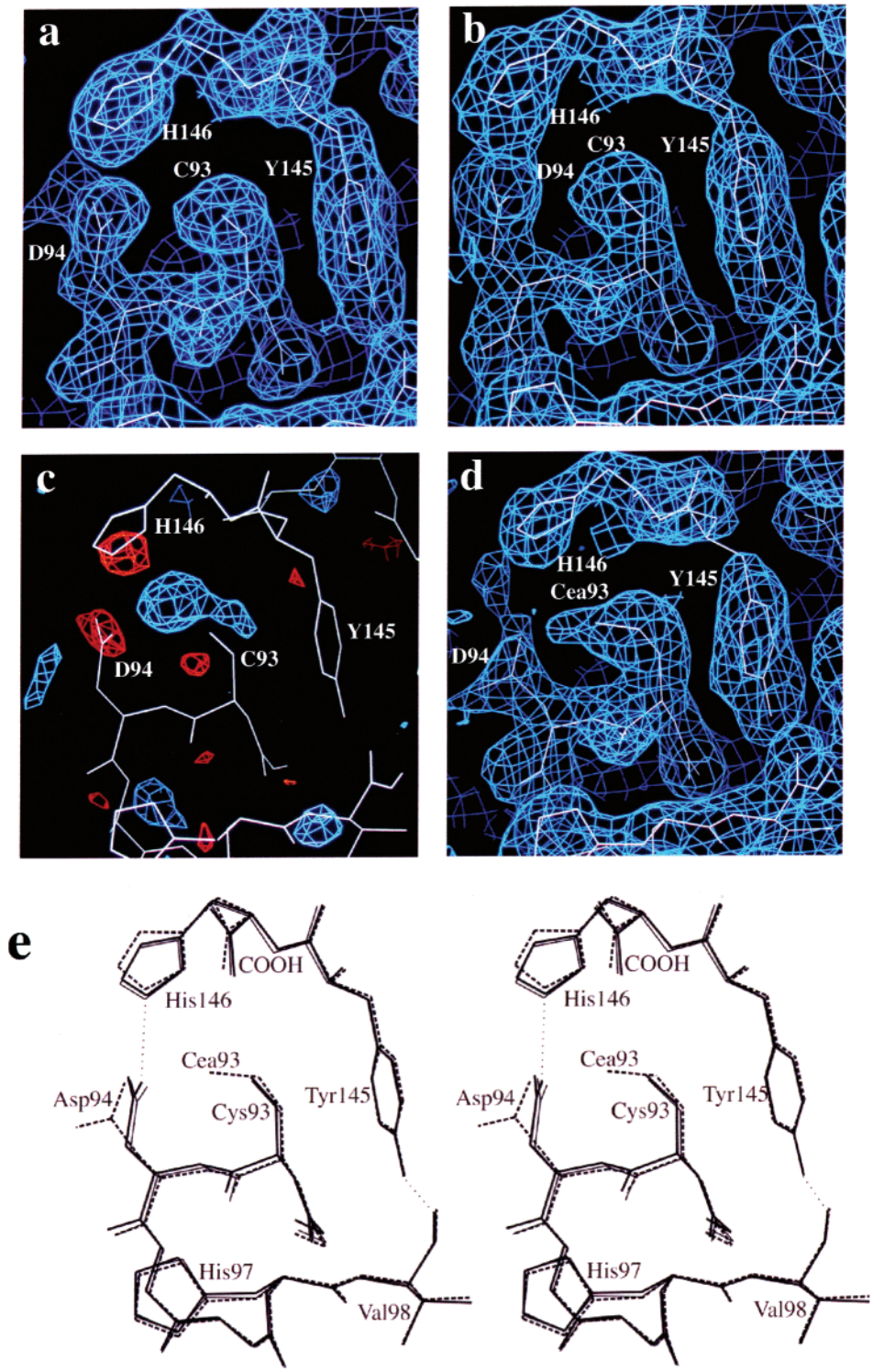

FIGURE 7: $2F_o - F_c$ electron density maps showing the environment of Cys93(F9)β1 for (a) deoxyhemoglobin, (b) quaternary-T nitrosylhemoglobin under anaerobic conditions, and (d) quaternary-T nitrosylhemoglobin under aerobic conditions. Residues Cys93(F9)β1, Asp94(FG1)β1, Tyr145(HC2)β1, and His146(HC3)β1 were not included in the atomic model used to calculate the F_c structure factor magnitudes and phases. The electron density contours are drawn at 1.6 times the rms density of the map. (c) $F_{\text{aerobic T nitrosylhemoglobin}} - F_{\text{anaerobic T nitrosylhemoglobin}}$ difference electron density map calculated with phases derived from the refined structure of the anaerobic quaternary-T nitrosylhemoglobin. The positive (blue) and negative (red) difference electron density contours are drawn at + 3.0 and −3.0 times the rms density of the map. (e) Stereo diagram showing the environment of the Cys93(F9)β1 in deoxyhemoglobin (thin lines), quaternary-T nitrosylhemoglobin under anaerobic conditions (thick lines), and quaternary-T nitrosylhemoglobin under aerobic conditions (dashed lines) after the nitrosylhemoglobin structures were superimposed on the deoxyhemoglobin structure. In panels d and e, Cea93 refers to Cys93-(F9)β1 sulfenic acid.

study of NO-associated modification of cysteine in a protein other than hemoglobin [the crystal structure of glutathione reductase inactivated by reaction with the NO carriers *S*-nitrosoglutathione and (diglutathionyldinitroso)iron] resulted in the production of cysteinesulfinic acid (Cys-SO_2H) and cysteinesulfenic acid (*58*).

In contrast to our crystallographic study on the reaction of NO with quaternary-T hemoglobin under anaerobic conditions, our virtually identical study on the reaction of NO with quaternary-R2 carbonmonoxyhemoglobin under anaerobic conditions showed clear evidence of a NO reaction product at Cys93(F9)β (*26*). Since this result contradicted the solution studies noted above, we speculated that transiently formed methemoglobin or possibly contaminants, such as O_2, other nitrogen oxides, or metal ions, may have served as an electron acceptor to promote the S-nitrosylation reaction. With this caveat, we modeled the Cys93(F9)β adduct as Cys-SNO because the very well defined electron density adjacent to the sulfur atom had the size and shape to accommodate two additional atoms (*26*). Subsequently, Bartberger et al. (*59*) reported spectroscopic and small molecule crystallographic data, supported by theoretical computations, that showed the S−N bond in *S*-nitrosothiols must have significant double bond character. That is, the C−S−N−O dihedral angle should adopt a value of ∼0° (the syn conformation) or ∼180° (the anti conformation). However, in our refined structure of SNO-nitrosylhemoglobin, the C−S−N−O dihedral angle for SNO-Cys93(F9)β has a value of ∼80°. Despite repeated efforts to re-refine this 1.8 Å crystal structure without stereochemical restraints that would bias the C−S−N−O dihedral angle, we have been unable to fit the electron density of the SNO-Cys93(F9)β adduct with an atomic model that has either a syn or an anti conformation. All of these efforts resulted in C−S−N−O dihedral angles between 70° and 90° for SNO-Cys93(F9)β1 and SNO-Cys93(F9)β2.

A solution to the apparent inconsistencies between our crystal structure of quaternary-R2 SNO-nitrosylhemoglobin and the published studies described above is provided by the work of Gow et al. (*30*) and DeMaster et al. (*60*) on the reaction mechanism of NO with free sulfhydryl groups. Both groups have reported evidence for the formation of the radical intermediate Cys-S−N$^{\bullet}$−O−H in the absence of O_2. If, under our experimental conditions (i.e., an anaerobic environment and a very high free NO concentration), the Cys-S−N$^{\bullet}$−O−H radical is stabilized in quaternary-R2 hemoglobin, then this would explain the nonplanarity of the C−S−N−O group in our atomic model of quaternary-R2 SNO-nitrosylhemoglobin. Moreover, if the electron density associated with the Cys93(F9)β adduct in our SNO-nitrosylhemoglobin crystal structure is modeled as the Cys-S−N$^{\bullet}$−O−H radical, another potential stereochemical problem is resolved. In our published structure of SNO-nitrosylhemoglobin the distance between the *S*-nitrosothiol oxygen atom and the carbonyl oxygen of Val98(FG5)β is ∼3.0 Å, a distance that is unusually short for an O···O noncovalent contact. A Cys-S−N$^{\bullet}$−O−H radical, on the other hand, would form an energetically favorable hydrogen bond with the carbonyl oxygen of Val98(FG5)β at this distance. Thus, we suggest that in the quaternary-R2 conformation (and in the quaternary-R^e ensemble, in general, where Cys93(F9)β is similarly oriented) the orientation and environment of the Cys93(F9)β sulfhydryl serve to stabilize the Cys-S−N$^{\bullet}$−O−H radical. In the quaternary-T conformation, where the Cys93(F9)β sulfhydryl is oriented away from Val98(FG5)β and toward the solvent, the Cys-S−N$^{\bullet}$−O−H radical would not be stabilized. By stabilizing the Cys-S−N$^{\bullet}$−O−H intermediate, the environment of Cys93(F9)β in the quaternary-R^e ensemble should promote the subsequent reaction with O_2 to form the final *S*-nitrosothiol product (*30*). This factor, together with the energetically costly disruption of the Asp94(FG1)β···His146(HC3)β salt bridge that is required in the quaternary-T conformation, provides a stereochemical explanation for the greater reactivity of Cys93(F9)β with NO in liganded hemoglobin.

In Quaternary-T Hemoglobin Ligand Binding Induces Tension in the α*-Heme−Globin Linkage*. The issue of how quaternary constraints control the ligand affinity of the α-subunits was outlined initially in a theory advanced by Perutz. Beginning in 1972, Perutz and co-workers proposed that the low oxygen affinity of quaternary-T hemoglobin is a consequence of tension in the Fe−histidine bonds (*8*−*11*). Subsequently, several spectroscopic studies of nitrosylhemoglobin verified this proposal and demonstrated that most of Fe−histidine tension is a consequence of ligand-induced tension in the Fe−N$^{\epsilon}$His87(F8)α bond and not the Fe−N$^{\epsilon}$His92(F8)β bond (*1*−*3*). In particular, through the use of UV, visible, IR, CD, and ESR spectroscopy, it was determined that in the absence of IHP the α- and β-heme groups of nitrosylhemoglobin are six-coordinate, just as they are in fully liganded oxyhemoglobin or carbonmonoxyhemoglobin. In contrast, it was determined that the addition of IHP shifts the quaternary structure of nitrosylhemoglobin from the R^e ensemble to the quaternary-T conformation in which the two Fe−N$^{\epsilon}$His87(F8)α bonds are ruptured (*1*−*3*). Both the Fe−N$^{\epsilon}$His87(F8)α and the Fe−N$^{\epsilon}$His92(F8)β bonds should be weakened in nitrosylhemoglobin (but not in oxy- or carbonmonoxyhemoglobin) because of the strong repulsive trans effect generated by the unpaired electron of the axial NO ligand (*61*). Since the Fe−N$^{\epsilon}$His87(F8)α bond, but not the Fe−N$^{\epsilon}$His92(F8)β bond, is broken in the IHP−nitrosylhemoglobin complex, this implies that ligand binding to the quaternary-T hemoglobin tetramer induces a high level of tension in the Fe−N$^{\epsilon}$His87(F8)α bond but not (or to a much lesser degree) in the Fe−N$^{\epsilon}$His92(F8)β bond. Thus, in solution, IHP greatly stabilizes the quaternary-T structure of nitrosylhemoglobin where the Fe−N$^{\epsilon}$His87(F8)α bond is broken and prevents transition to the R^e ensemble of quaternary structures where the Fe−N$^{\epsilon}$His87(F8)α bond is intact. Likewise, the crystallographic results described above demonstrate that relatively weak crystal lattice contacts also can stabilize nitrosylhemoglobin in the quaternary-T structure with ruptured Fe−N$^{\epsilon}$His87(F8)α bonds and prevent transition to the R^e ensemble of quaternary structures with intact Fe−N$^{\epsilon}$His87(F8)α bonds. The same observation was made by Paoli et al. (using the same crystal form of hemoglobin) in the case of quaternary-T cyanomethemoglobin (*12*). In contrast, this crystal form of deoxyhemoglobin cracks and disorders when exposed to CO or O_2, presumably because the Fe−N$^{\epsilon}$His87(F8)α bonds remain intact and the ligand-induced tension is relieved not by bond breaking but by triggering the T−R^e transition.

Also consistent with the central role of the Fe−N$^{\epsilon}$His87(F8)α bond in triggering the ligation-induced T−R^e transition are other published experiments in which the covalent tethers between the α- and β-globins and the heme groups are selectively eliminated. In particular, "proximal detachment" studies carried out by Barrick et al. specifically eliminated the linkage between the α-heme and His87(F8)α and/or the

β-heme and His92(F8)β by effectively removing the β-methylene groups of the proximal histidines (*62*, *63*). In these studies, the mutations αH87G and βH92G were created so that the normal histidine side chain could be replaced with a heme-linked imidazole group that is not covalently attached to the globin backbone. These researchers found that when the proximal linkage between the globin and the heme is broken in the α-subunits, the fully liganded tetramer maintains CD, near-UV, and ^{1}H NMR spectroscopic signatures characteristic of the quaternary-T tetramer. However, when the proximal linkage between the globin and the heme is broken in the β-subunits, but not in the α-subunits, the spectroscopic data indicate that the T$-$R^e transition occurs. Together, the nitrosylhemoglobin studies and the proximal detachment studies show that in quaternary-T hemoglobin the α-heme$-$globin linkage is essential for the ligation-induced disruption of quaternary constraints and initiation of the T$-$R^e transition. A number of other experiments involving heme groups with non-Fe metal atoms, or without a central metal atom, are also consistent with the Fe$-$N$^\epsilon$-His87(F8)α bond having a more significant role in triggering the T$-$R^e transition (*64*$-$*68*).

The Structure of Quaternary-T βW37E Nitrosylhemoglobin Directly Demonstrates the Link between Quaternary Constraints and Ligand-Induced Tension in the Fe$-$N$^\epsilon$His87(F8)α Bond. Hemoglobin's allosteric properties are due to quaternary structure interactions (quaternary constraints) that form when two $\alpha\beta$ dimers, that have very high ligand affinity, assemble to generate an $\alpha_2\beta_2$ tetramer with low ligand affinity. Precise thermodynamic measurements by Ackers et al. (*69*) have determined that the affinity difference between dimers and tetramers amounts to a factor of $\sim$400 in the case of O_2 binding. This implies that the interdimer interactions that form between the two $\alpha\beta$ dimers lower the ligand affinity of the tetramer by resisting tertiary structure changes that are induced by ligand binding. An understanding of hemoglobin's mechanism of action involves, therefore, the detailed delineation of two key issues: (1) identification of the quaternary constraints and (2) determining how these dimer$-$dimer interactions act to lower the ligand affinity of the α- and β-heme groups.

The issue of quaternary constraint identification has been addressed most recently by Noble et al. (*13*). In theory, the particular residues that constitute the quaternary constraints could be distributed over the entire dimer$-$dimer interface, or they could be confined to a small region of the interface. By coupling the use CO-combination kinetic measurements and oxygen equilibrium studies (in solution and in hemoglobin crystals) with an extensive mutagenic screen of the dimer$-$dimer interface, Noble et al. have provided convincing evidence that most of the quaternary constraints are localized to a small cluster of residues that are centered on residue Trp37(C3)β. Mutations such as βW37G and βW37E eliminate almost all of the quaternary constraints associated with the quaternary-T tetramer (*13*$-$*17*). In addition, mutations of residues that are in direct contact with Trp37(C3)β [e.g., Arg92(FG4)α, Asp94(G1)α, Pro95(G2)α, Tyr140(HC2)β, Arg141(HC3)β, Tyr35(C1)β, and Pro36(C2)β] also result in a significant reduction of the quaternary constraints associated with the quaternary-T tetramer (*13*). This group of residues, referred to as the β37 cluster, is located in the so-called "hinge region" of the $\alpha1\beta2$ interface.

Exposing crystals of the mutant deoxyhemoglobin βW37E to NO offers a clear-cut test of the hypothesis that there is a direct link between ligand-induced tension in the Fe$-$N$^\epsilon$-His87(F8)α bond and the quaternary constraints in the β37 cluster. That is, if such a linkage exists, then the Fe$-$N$^\epsilon$-His87(F8)α bond should remain intact when crystals of βW37E deoxyhemoglobin are exposed to NO. Conversely, if this direct link does not exist, the Fe$-$N$^\epsilon$His87(F8)α bond should rupture in crystals of βW37E deoxyhemoglobin exposed to NO as it does in wild-type crystals of deoxyhemoglobin that are exposed to NO. Since we found the Fe$-$N$^\epsilon$His87(F8)α bond to be intact in quaternary-T βW37E nitrosylhemoglobin, we can conclude that there is in fact a direct stereochemical linkage between ligand-induced tension in the Fe$-$N$^\epsilon$His87(F8)α bond and the quaternary constraints in the β37 cluster.

Stereochemical Relationships between Quaternary Constraints and Ligand-Induced Tertiary Structure Changes. Perutz (*55*, *70*) has outlined a stereochemical mechanism that suggests how ligand-induced tertiary structure changes trigger a quaternary transition from the low-affinity quaternary-T structure to the high-affinity quaternary-R structure. A key tenet of Perutz's mechanism is that "...each subunit can take up only two alternate stable tertiary structures, the deoxy and the liganded form," and that "...these two structures may be subject to strains when subunits are confined to the 'wrong' quaternary structure" (*55*). In the case of the α-subunits, Perutz proposed that a ligand-induced movement of the heme Fe atom into the heme plane causes the proximal histidine and F-helix to shift in a way that forces Tyr140(HC2)α out of its pocket between the F- and H-helices and ruptures the intersubunit salt bridges between Arg141(HC3)α1 and Asp126(H9)α2 and Lys127(H1)α2. In fact, comparison of deoxyhemoglobin and quaternary-T βW37E nitrosylhemoglobin electron density images clearly shows that NO binding displaces Tyr140(HC2)α (see Figures 1a and 6a) and disrupts the Arg141(HC3)α salt bridges within the quaternary-T structure. Although these salt bridges are important quaternary constraints, as Perutz proposed, more recent research (*13*$-$*17*, *49*) shows that the intersubunit interactions associated with Arg141(HC3)α constitute only a portion of the network of interactions centered at Trp37(C3)β that collectively function to reduce the ligand affinity of the deoxyhemoglobin tetramer. Within this cluster, mutations at Trp37(C3)β and Tyr140(HC2)α actually have the greatest impact on the allosteric properties of deoxyhemoglobin (*13*).

Perutz proposed that steric hindrance between the ligand and residues in the β distal pocket is the basis for the reduced ligand affinity of the β-subunits in quaternary-T hemoglobin (*55*, *70*). In particular, he proposed that in the quaternary-R structure ligand binding is unhindered, but in the quaternary-T structure the β-heme pocket narrows such that close contacts develop between the ligand and Val67(E11)β and His63(E7)β. Our crystallographic study of NO binding to crystalline quaternary-T hemoglobin reveals a series of six ligand-induced changes in tertiary structure that cross-validate (features 1β through 6β in Figure 3). Only one of these structural changes (feature 3β) corresponds to the widening of the heme pocket due to direct steric contacts between the ligand and the protein. Another structural change (feature 1β) is an indirect effect of steric contacts between the ligand

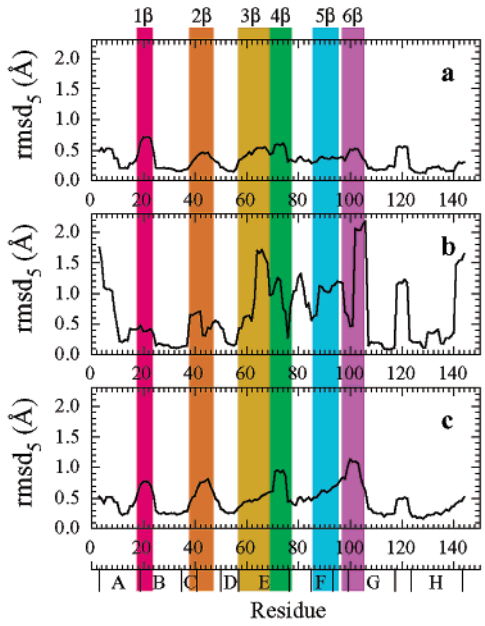

FIGURE 8: Plots of β-subunit rmsd$_5$ profiles of (a) quaternary-T nitrosylhemoglobin versus quaternary-T deoxyhemoglobin, (b) horse quaternary-R BME-deoxyhemoglobin versus horse quaternary-R carbonmonoxyhemoglobin, and (c) quaternary-T βW37E nitrosylhemoglobin versus quaternary-T deoxyhemoglobin. All profiles are plotted on the same scale. The profiles in panels a and c are averages of the β1 and β2 profiles. The profile in panel a is the average of the β1 and β2 profiles shown in Figure 3a plotted on the expanded scale. Since the asymmetric unit in horse quaternary-R methemoglobin crystals is a single $\alpha\beta$ dimer, the β1 and β2 profiles are identical.

and the protein. The remaining four regions of structural change (features 2β, 4β, 5β, and 6β) are the result of a ligand-induced shift of the heme group. Since these β-subunit tertiary structure changes, which occur within the quaternary-T conformation, appear to be due to internal perturbations involving globin−heme contacts and globin−ligand contacts, it is reasonable to expect that they would also occur within any of the R^e ensemble quaternary conformations. That is, a similar pattern of β-subunit tertiary structure changes should be observed in a comparison between deoxy and liganded β-subunits within the R^e ensemble. The recent publication of the high-resolution structure of bis(*N*-maleimidoethyl)-modified horse deoxyhemoglobin (BME-deoxyhemoglobin) provides an opportunity to test this prediction (*71*). The bifunctional BME reagent reacts with Cys93(F9)β (and perhaps a second residue) and stabilizes the modified crystalline deoxyhemoglobin in the quaternary-R conformation. In Figure 8, panels a and b show rmsd$_5$ profiles of quaternary-T nitrosylhemoglobin versus quaternary-T deoxyhemoglobin and of horse quaternary-R BME-deoxyhemoglobin versus horse quaternary-R carbonmonoxyhemoglobin, respectively. Comparison of these two profiles shows that the six cross-validated, ligand-induced tertiary structure changes identified in the quaternary-T tetramer (features 1β through 6β) occur in the quaternary-R tetramer as well and, therefore, are intrinsic to the β-subunits. However, the magnitudes of features 1β and 2β do not change, while features 3β through 6β are significantly larger in the quaternary-R profile and, therefore, must be linked to the quaternary-T constraints. The quaternary-R profile also contains a few additional features, and these may be linked to the quaternary-T constraints as well. (Curiously, one of the additional features corresponds to a feature that did not cross-validate in our analysis of quaternary-T nitrosylhemoglobin. The reason for this discrepancy is not yet clear.) Thus, consistent with Perutz's tenet, the quaternary constraints in the dimer−dimer interface of the quaternary-T tetramer are limiting the relaxation of ligand-induced β-subunit tertiary structure changes. Also consistent with this general principle is the finding that the magnitudes of the ligand-induced tertiary structure changes increase when the quaternary-T constraints are greatly reduced by the βW37E mutation (Figure 8c). The question of exactly how the β-subunit ligand-induced tertiary structure changes are linked to the dimer−dimer quaternary-T constraints (i.e., the β37 cluster) remains to be determined.

REFERENCES

1. Maxwell, J. C., and Caughey, W. S. (1976) *Biochemistry 15*, 388−396.
2. Szabo, A., and Perutz, M. F. (1976) *Biochemistry 15*, 4427−4428.
3. Hille, R., Olson, J. S., and Palmer, G. (1979) *J. Biol. Chem. 254*, 12110−12120.
4. Mueser, T. C., Rogers, P. H., and Arnone, A. (2000) *Biochemistry 39*, 15353−15364.
5. Shaanan, B. (1983) *J. Mol. Biol. 171*, 31−59.
6. Silva, M. M., Rogers, P. H., and Arnone, A. (1992) *J. Biol. Chem. 267*, 17248−17256.
7. Lukin, J. A., Kontaxis, G., Simplaceanu, V., Yuan, Y., Bax, A., and Ho, C. (2003) *Proc. Natl. Acad. Sci. U.S.A. 100*, 517−520.
8. Perutz, M. F., Fersht, A. R., Simon, S. R., and Roberts, G. C. (1974) *Biochemistry 13*, 2174−2186.
9. Perutz, M. F., Heidner, E. J., Ladner, J. E., Beetlestone, J. G., Ho, C., and Slade, E. F. (1974) *Biochemistry 13*, 2187−2200.
10. Perutz, M. F., Ladner, J. E., Simon, S. R., and Ho, C. (1974) *Biochemistry 13*, 2163−2173.
11. Perutz, M. F. (1972) *Nature 237*, 495−499.
12. Paoli, M., Dodson, G., Liddington, R. C., and Wilkinson, A. J. (1997) *J. Mol. Biol. 271*, 161−167.
13. Noble, R. W., Hui, H. L., Kwiatkowski, L. D., Paily, P., DeYoung, A., Wierzba, A., Colby, J. E., Bruno, S., and Mozzarelli, A. (2001) *Biochemistry 40*, 12357−12368.
14. Kwiatkowski, L. D., Hui, H. L., Wierzba, A., Noble, R. W., Walder, R. Y., Peterson, E. S., Sligar, S. G., and Sanders, K. E. (1998) *Biochemistry 37*, 4325−4335.
15. Kiger, L., Klinger, A. L., Kwiatkowski, L. D., De Young, A., Doyle, M. L., Holt, J. M., Noble, R. W., and Ackers, G. K. (1998) *Biochemistry 37*, 4336−4345.
16. Peterson, E. S., and Friedman, J. M. (1998) *Biochemistry 37*, 4346−4357.
17. Kavanaugh, J. S., Weydert, J. A., Rogers, P. H., and Arnone, A. (1998) *Biochemistry 37*, 4358−4373.
18. Jia, L., Bonaventura, C., Bonaventura, J., and Stamler, J. S. (1996) *Nature 380*, 221−226.
19. Stamler, J. S., Jia, L., Eu, J. P., McMahon, T. J., Demchenko, I. T., Bonaventura, J., Gernert, K., and Piantadosi, C. A. (1997) *Science 276*, 2034−2037.
20. McMahon, T. J., Moon, R. E., Luschinger, B. P., Carraway, M. S., Stone, A. E., Stolp, B. W., Gow, A. J., Pawloski, J. R., Watke, P., Singel, D. J., Piantadosi, C. A., and Stamler, J. S. (2002) *Nat. Med. 8*, 711−717.
21. Patel, R. P., Hogg, N., Spencer, N. Y., Kalyanaraman, B., Matalon, S., and Darley-Usmar, V. M. (1999) *J. Biol. Chem. 274*, 15487−15492.
22. McMahon, T. J., Exton Stone, A., Bonaventura, J., Singel, D. J., and Solomon Stamler, J. (2000) *J. Biol. Chem. 275*, 16738−16745.
23. Hobbs, A. J., Galdwin, M. T., Patel, R. P., Williams, D. L. H., and Butler, A. R. (2002) *Trends Pharmacol. Sci. 23*, 406−411.
24. Stamler, J. S., Hess, D. T., and Singel, D. J. (2003) *Nat. Med. 9*, 42−43.
25. Rassaf, T., Bryan, N. S., Maloney, R. E., Specian, V., Kelm, M., Kalyanaraman, B., Rodriguez, J., and Feelisch, M. (2003) *Nat. Med. 9*, 481−482.
26. Chan, N.-L., Rogers, P. H., and Arnone, A. (1998) *Biochemistry 37*, 16459−16464.

27. Ward, K. B., Wishner, B. C., Lattman, E. E., and Love, W. E. (1975) *J. Mol. Biol. 98*, 161−177.
28. Kavanaugh, J. S., Rogers, P. H., Case, D. A., and Arnone, A. (1992) *Biochemistry 31*, 4111−4121.
29. Moore, E. G., and Gibson, Q. H. (1976) *J. Biol. Chem. 251*, 2788−2794.
30. Gow, A. J., Buerk, D. G., and Ischiropoulos, H. (1997) *J. Biol. Chem. 272*, 2841−2845.
31. Herold, S., and Rock, G. (2003) *J. Biol. Chem. 278*, 6623−6634.
32. Luchsinger, B. P., Rich, E. N., Gow, A. J., Williams, E. M., Stamler, J. S., and Singel, D. J. (2003) *Proc. Natl. Acad. Sci. U.S.A. 100*, 461−466.
33. Liddington, R. (1994) *Methods Enzymol. 232*, 15−26.
34. Waller, D. A., and Liddington, R. C. (1990) *Acta Crystallogr. B46*, 409−418.
35. Howard, A. J., Nielsen, C., and Xuong, N. H. (1985) *Methods Enzymol. 114*, 452−472.
36. Brünger, A. T. (1992) *X-PLOR, version 3.1*, Yale University Press, New Haven, CT.
37. Hendrickson, W. A. (1985) *Methods Enzymol. 115*, 252−270.
38. Murshudov, G., Vagin, A. A., and Dodson, E. J. (1997) *Acta Crystallogr. D53*, 240−255.
39. Collaborative Computational Project (1994) *Acta Crystallogr. D50*, 760−763.
40. Jones, T. A. (1985) *Methods Enzymol. 115*, 157−171.
41. Cambillau, C. (1989) *Silicon Graphics Geometry Partners Directory*, p 61, Silicon Graphics, Mountain View, CA.
42. Arnone, A., and Perutz, M. F. (1974) *Nature 249*, 34−36.
43. Brünger, A. T. (1992) *Nature 355*, 472−474.
44. Brünger, A. T. (1993) *Acta Crystallogr. D49*, 24−36.
45. Gerstein, M., and Chothia, C. (1991) *J. Mol. Biol. 220*, 133−149.
46. Perutz, M. F., Kilmartin, J. V., Nagai, K., Szabo, A., and Simon, S. R. (1976) *Biochemistry 15*, 378−387.
47. Taketa, F., Antholine, W. E., and Chen, J. Y. (1978) *J. Biol. Chem. 253*, 5448−5451.
48. Scheidt, W. R., and Piciulo, P. L. (1976) *J. Am. Chem. Soc. 98*, 1913−1919.
49. Kavanaugh, J. S., Chafin, D. R., Arnone, A., Mozzarelli, A., Rivetti, C., Rossi, G. L., Kwiatkowski, L. D., and Noble, R. W. (1995) *J. Mol. Biol. 248*, 136−150.
50. Brucker, E. A., Olson, J. S., Ikeda-Saito, M., and Phillips, G. N. J. (1998) *Proteins 30*, 352−356.
51. Harutyunyan, E. H., Safonova, T. N., Kuranova, I. P., Popov, A. N., Teplyakov, A. V., Obmolova, G. V., Valnshtein, B. K., Dodson, G. G., and Wilson, J. C. (1996) *J. Mol. Biol. 264*, 152−161.
52. Baldwin, J., and Chothia, C. (1979) *J. Mol. Biol. 129*, 175−220.
53. Paoli, M., Liddington, R., Tame, J., Wilkinson, A., and Dodson, G. (1996) *J. Mol. Biol. 256*, 775−792.
54. Cox, J. M. (1967) *J. Mol. Biol. 28*, 151−156.
55. Perutz, M. F. (1970) *Nature 228*, 726−739.
56. Perutz, M. F. (1979) *Annu. Rev. Biochem. 48*, 327−386.
57. Kharitonov, V. G., Sundquist, A. R., and Sharma, V. S. (1995) *J. Biol. Chem. 270*, 28158−28164.
58. Becker, K., Savvides, S. N., Keese, M., Schirmer, R. H., and Karplus, P. A. (1998) *Nat. Struct. Biol. 5*, 267−271.
59. Bartberger, M. D., Houk, K. N., Powell, S. C., Mannion, J. D., Lo, K. Y., Stamler, J. S., and Toone, E. J. (2000) *J. Am. Chem. Soc. 122*, 5889−5890.
60. DeMaster, E. G., Quast, B. J., Redfern, B., and Nagasawa, H. T. (1995) *Biochemistry 34*, 11494−11499.
61. Decatur, S. M., Franzen, S., DePillis, G. D., Dyer, R. B., Woodruff, W. H., and Boxer, S. G. (1996) *Biochemistry 35*, 4939−4944.
62. Barrick, D., Ho, N. T., Simplaceanu, V., Dahlquist, F. W., and Ho, C. (1997) *Nat. Struct. Biol. 4*, 78−83.
63. Barrick, D., Ho, N. T., Simplaceanu, V., and Ho, C. (2001) *Biochemistry 40*, 3780−3795.
64. Shibayama, N., Inubushi, T., Morimoto, H., and Yonetani, T. (1987) *Biochemistry 26*, 2194−2201.
65. Shibayama, N., Yonetani, T., Regan, R. M., and Gibson, Q. H. (1995) *Biochemistry 34*, 14658−14667.
66. Fujii, M., Hori, H., Miyazaki, G., Morimoto, H., and Yonetani, T. (1993) *J. Biol. Chem. 268*, 15386−15393.
67. Nagatomo, S., Nagai, M., Tsuneshige, A., Yonetani, T., and Kitagawa, T. (1999) *Biochemistry 38*, 9659−9666.
68. Nagatomo, S., Nagai, M., Shibayama, N., and Kitagawa, T. (2002) *Biochemistry 41*, 10010−10020.
69. Ackers, G. K., Holt, J. M., Huang, Y., Grinkova, Y., Klinger, A. L., and Denisov, I. (2000) *Proteins, Suppl.*, 23−43.
70. Perutz, M. F., Wilkinson, A. J., Paoli, M., and Dodson, G. G. (1998) *Annu. Rev. Biophys. Biomol. Struct. 27*, 1−34.
71. Wilson, J., Phillips, K., and Luisi, B. (1996) *J. Mol. Biol. 264*, 743−756.
72. Scheidt, W. R., and Frisse, M. E. (1975) *J. Am. Chem. Soc. 97*, 17−21.

BI030172J